

A hydrodynamic model of Alfvénic waves and fast magneto-sound in the relativistically hot plasmas at propagation parallel to the magnetic field

Pavel A. Andreev*

*Department of General Physics, Faculty of physics,
Lomonosov Moscow State University, Moscow, Russian Federation, 119991. and
Peoples Friendship University of Russia (RUDN University),
6 Miklukho-Maklaya Street, Moscow, 117198, Russian Federation*

(Dated: August 31, 2021)

The Alfvénic waves and fast magneto-sound in the relativistically hot plasmas are considered. This study is based on the novel hydrodynamic model of plasmas with the relativistic temperatures consisted of four equations for the material fields: the concentration and the velocity field *and* the average reverse relativistic γ functor and the flux of the reverse relativistic γ functor. Three temperature regimes giving considerably different behavior of the spectrum of Alfvénic waves are found. Four temperature regimes are obtained for the fast magneto-sound. All these regimes show considerable variations from the nonrelativistic regime. Dispersion equations for the electromagnetic transverse wave propagating parallel to the external magnetic field are found analytically. Their small frequency solutions are analyzed numerically.

Keywords: relativistic plasmas, hydrodynamics, microscopic model, arbitrary temperatures

I. INTRODUCTION

The low frequency transverse electromagnetic waves (the Alfvénic waves and fast magneto-sound) play essential role in many processes in laboratory plasmas and space plasmas [1], [2], [3], [4], [5], [6], [7], [8], [9], [10], [11], [12], [13], [14], [15], [16]. These fundamental waves are important for the low temperature plasmas and the relativistically hot plasmas. There are the hydrodynamic approaches to the relativistically hot plasmas [17], [18], [19], [20], [21]. However, we apply the recently suggested hydrodynamic model [22], which is also applied to other wave phenomena [23], [24].

The model presented below can be derived by various technics. But, we present basic definitions appearing at the direct derivation of hydrodynamics from the microscopic mechanic motion in accordance with Ref. [22], where this set of equations is suggested for the description of the relativistic plasmas.

We use an explicit form of operator giving the transition from the microscopic scale to the macroscopic scale. We illustrate it with the presentation of the concentration of particles $n(\mathbf{r}, t)$ in the arbitrary inertial frame [22]

$$n(\mathbf{r}, t) = \frac{1}{\Delta} \int_{\Delta} d\xi \sum_{i=1}^N \delta(\mathbf{r} + \xi - \mathbf{r}_i(t)). \quad (1)$$

This definition is suggested in Refs. [25], [26], [27]. Non-relativistic plasmas are considered in Refs. [26], [27]. More general concept as a background of the relativistic kinetics is given in Ref. [25]. Presented description is a generalization of the Klimontovich method [28], where the method of transition to the macroscopic level is presented via unspecified averaging.

Following the evolution of concentration $n(\mathbf{r}, t)$ (1) we obtain the continuity equation together with the microscopic definition of the current of particles, which is traditionally represented via the velocity field. Next step is the derivation of the current of particles. This equation gives additional functions together with their microscopic definitions. Kinematic part of the evolution of the current of particles gives the flux of the current of particles. The dynamical part presented within the electromagnetic field. It is considered in the mean-field (the self-consistent field) approximation. Hence, three additional functions appear. They are the average reverse relativistic γ functor, the flux of the reverse relativistic γ functor, and the second rank tensor of the current of the flux of the reverse relativistic γ functor. Further extension of the set of hydrodynamic equations includes the equations for evolution of the average reverse relativistic γ functor and the flux of the reverse relativistic γ functor. The higher rank tensors are represented via the functions of smaller tensor rank using equations of state [22].

This paper is organized as follows. In Sec. II the relativistic hydrodynamic equations are demonstrated. In Sec. III the spectra of Alfvénic waves and fast magneto-sound are obtained and analyzed. In Sec. IV a brief summary of obtained results is presented.

II. RELATIVISTIC HYDRODYNAMIC MODEL

The hydrodynamic equations for the relativistic plasmas with the relativistic temperature [22] are applied here to study the spectrum of Alfvénic waves and fast magneto-sound. The relativistic hydrodynamic model consists of four equations (in three-vector notations). First equation is the continuity equation

$$\partial_t n_s + \nabla \cdot (n_s \mathbf{v}_s) = 0, \quad (2)$$

*Electronic address: andreevpa@physics.msu.ru

where $s = e, i$ is the index showing the species of electrons and ions. The continuity equation does not contain any contribution of interaction. The dynamics of concentration n depend on the evolution of the velocity field. So, we need to present the equation for the velocity field evolving with time. Let us mention that the velocity field is proportional to the current of particles. It has no simple relation with the momentum density. Following Ref. [22] we present the velocity field evolution equation:

$$m_s n_s [\partial_t v_s^a + (\mathbf{v}_s \cdot \nabla) v_s^a] + \partial^a p_s = q_s \Gamma_s E^a$$

$$+ \frac{q_s}{c} \varepsilon^{abc} (\Gamma_s v_s^b + t_s^b) B^c - \frac{q_s}{c^2} [(\Gamma_s v_s^a v_s^b + v_s^a t_s^b + v_s^b t_s^a) E^b + \tilde{t}_s E^a], \quad (3)$$

where p_s is the flux of the thermal velocities. The interaction is found in the mean-field approximation. The equation of evolution of the averaged reverse relativistic gamma factor, called here the hydrodynamic Gamma function, is

$$\partial_t \Gamma_s + \partial_b (\Gamma_s v_s^b + t_s^b) = - \frac{q_s n_s}{m_s c^2} \mathbf{v}_s \cdot \mathbf{E} \left(1 - \frac{1}{c^2} \left(\mathbf{v}_s^2 + \frac{5p_s}{n_s} \right) \right). \quad (4)$$

The averaged reverse relativistic gamma factor appears on the right-hand side of the velocity field evolution equation. It appears along with the vector of current of the reverse relativistic gamma factor and the second rank tensor describing the flux of current of the reverse relativistic gamma factor.

The fourth equation in the presented set of hydrodynamic equations is the equation for the thermal part of the current of the reverse relativistic gamma factor (thermal part of the hydrodynamic Theta function):

$$(\partial_t + \mathbf{v}_s \cdot \nabla) t_s^a + \partial_a \tilde{t}_s + (\mathbf{t}_s \cdot \nabla) v_s^a + t_s^a (\nabla \cdot \mathbf{v}_s)$$

$$+ \Gamma_s (\partial_t + \mathbf{v}_s \cdot \nabla) v_s^a = \frac{q_s}{m} n_s E^a \left[1 - \frac{\mathbf{v}_s^2}{c^2} - \frac{3p_s}{n_s c^2} \right]$$

$$+ \frac{q_s}{m_s c} \varepsilon^{abc} n_s v_s^b B^c \left[1 - \frac{\mathbf{v}_s^2}{c^2} - \frac{5p_s}{n_s c^2} \right] - \frac{2q_s}{m_s c^2} E^a p_s \left[1 - \frac{\mathbf{v}_s^2}{c^2} \right]$$

$$- \frac{q_s}{m_s c^2} n_s v_s^a v_s^b E^b \left[1 - \frac{\mathbf{v}_s^2}{c^2} - \frac{9p_s}{n_s c^2} \right] - \frac{10q_s}{3m_s c^4} M_s E^a. \quad (5)$$

The equations for the material fields (2)-(5) are coupled to the Maxwell equations $\nabla \cdot \mathbf{B} = 0$, $\nabla \times \mathbf{E} = -\frac{1}{c} \partial_t \mathbf{B}$,

$$\nabla \cdot \mathbf{E} = 4\pi(q_e n_e + q_i n_i), \quad (6)$$

and

$$\nabla \times \mathbf{B} = \frac{1}{c} \partial_t \mathbf{E} + \frac{4\pi q_e}{c} n_e \mathbf{v}_e + \frac{4\pi q_i}{c} n_i \mathbf{v}_i. \quad (7)$$

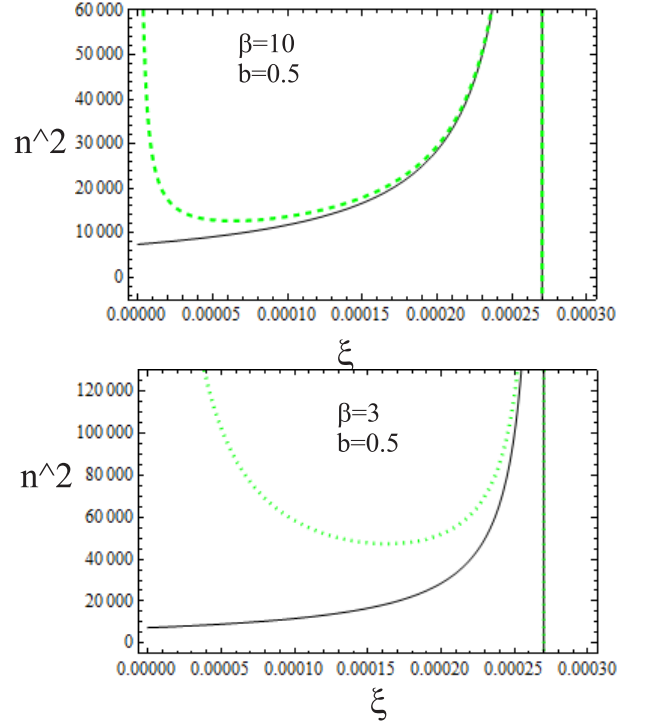


FIG. 1: The square of the refractive index of the Alfvénic waves is demonstrated. Each figure contains the square of the refractive index in relativistic regime with the temperature characterized by parameter $\beta = m_e c^2 / T$, which is plotted within the dashed green line. Plasmas under consideration are isothermal $T_e = T_i = T$. Temperature is given in the energy units. It is compared with the nonrelativistic regime presented within the black continuous line. Here we have two regimes corresponding to the relativistically hot electrons $T \sim m_e c^2$: $\beta = 10$ and $\beta = 3$. Due to the large mass of ions it corresponds to the nonrelativistic regime for ions. Large value of the parameter β (on the upper figure we have $\beta = 10$) corresponds to small relativistic effects for electrons.

III. ALFVENIC WAVES AND FAST MAGNETO-SOUND IN THE RELATIVISTICALLY HOT PLASMAS

High-frequency regime for the electromagnetic transverse wave propagating parallel to the external magnetic field is considered in Ref. [23], where the motion of ions is neglected. Here we consider the small-frequency excitations (Alfvénic waves and fast magneto-sound) in the relativistically hot plasmas and focus our attention on the contribution of ions.

We consider small amplitude collective excitations of the macroscopically motionless equilibrium state. This equilibrium state is described by the relativistic Maxwellian distribution. The equilibrium state is described within equilibrium concentrations $n_{0e} = n_{0i} \equiv n_0$. The velocity fields $\mathbf{v}_{0e,i}$ in the equilibrium state are equal to zero. The equilibrium electric field \mathbf{E}_0 is also equal to zero. The plasma is located in the constant and

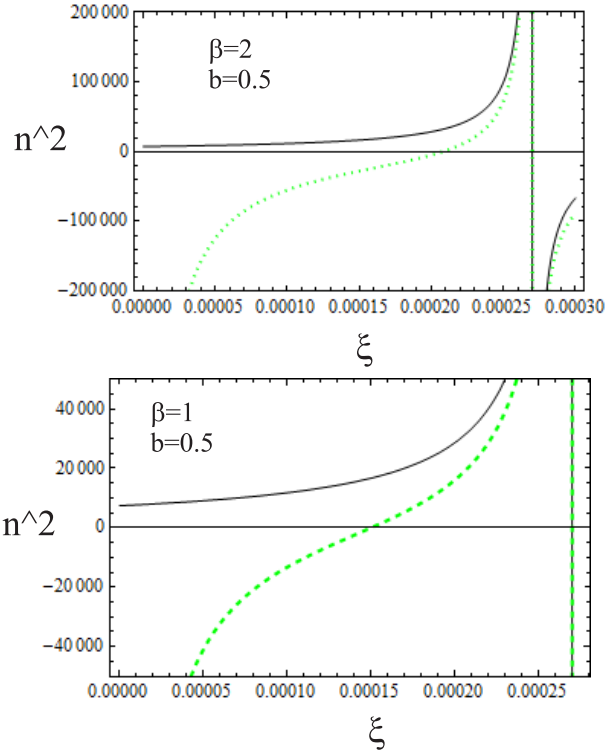


FIG. 2: The square of the refractive index of the Alfvénic waves is demonstrated. The further increase of temperature in compare with Fig. 1 is presented. Two temperatures are used for two plots in this figure $\beta = 2$ and $\beta = 1$.

uniform external magnetic field $\mathbf{B}_0 = B_0 \mathbf{e}_z$. Two second rank tensors and one fourth rank tensor are involved in the description of the thermal effects. The symmetric tensors $p_{e,i}^{ab}$ and $t_{e,i}^{ab}$ are assumed to be diagonal tensors: $p_{e,i}^{ab} = p_{e,i} \delta^{ab}$ and $t_{e,i}^{ab} = \tilde{t}_{e,i} \delta^{ab}$. The "diagonal" form is assumed for the symmetric fourth rank tensors $M_{e,i}^{abcd}$ as well: $M_{e,i}^{abcd} = M_{0e,i} (\delta^{ab} \delta^{cd} + \delta^{ac} \delta^{bd} + \delta^{ad} \delta^{bc})/3$.

The following equilibrium functions $\Gamma_{0e,i}$, $\mathbf{t}_{0e,i}$, $p_{0e,i}$, $\tilde{t}_{0e,i}$, $\mathbf{q}_{0e,i}$, $M_{0e,i}$ are involved in the description of the equilibrium state $p_{e,i}^{ab} = c^2 \delta^{ab} \tilde{Z}_{e,i} f_{1e,i}(\beta)/3$, $t_{e,i}^{ab} = c^2 \delta^{ab} \tilde{Z}_{e,i} f_{2e,i}(\beta)/3$, $M_{e,i}^{abcd} = c^4 (\delta^{ab} \delta^{cd} + \delta^{ac} \delta^{bd} + \delta^{ad} \delta^{bc}) \tilde{Z}_{e,i} f_{3e,i}(\beta)/15$, $\Gamma_{0e,i} = n_0 K_1(\chi_{e,i} \beta) / K_2(\chi_{e,i} \beta)$, $\chi_e = 1$, $\chi_i = (m_i/m_e) \cdot (T_e/T_i)$, and $\mathbf{q}_{e,i} = 0$, where $\beta = m_e c^2 / T_e$ is the reverse dimensionless temperature of electrons, $\tilde{Z}_{e,i} = 4\pi Z_{e,i} (m_{e,i} c)^3 = n_{e,i} \chi_{e,i} \beta K_2^{-1}(\chi_{e,i} \beta)$,

$$f_{1e,i}(\beta) = f_1(\chi_{e,i} \beta) = \int_1^{+\infty} \frac{dx}{x} (x^2 - 1)^{3/2} e^{-\chi_{e,i} \beta x}, \quad (8)$$

$$f_{2e,i}(\beta) = f_2(\chi_{e,i} \beta) = \int_1^{+\infty} \frac{dx}{x^2} (x^2 - 1)^{3/2} e^{-\chi_{e,i} \beta x}, \quad (9)$$

and

$$f_{3e,i}(\beta) = f_3(\chi_{e,i} \beta) = \int_1^{+\infty} \frac{dx}{x^3} (x^2 - 1)^{5/2} e^{-\chi_{e,i} \beta x}. \quad (10)$$

Factor χ_i shows representation of the dimensionless temperature of ions (in units of $m_i c^2$) via the dimensionless temperature of electrons (in units of $m_e c^2$). Functions $f_1(\beta)$, $f_2(\beta)$ and $f_3(\beta)$ are introduced in Ref. [22] for the electrons. Hence, dimensionless parameter x is the energy of electrons ε_e over the rest energy of electron $x = \varepsilon_e / m_e c^2$. Same functions for ions have different definition of the dimensionless parameter under integrals, where $x = \varepsilon_i / m_i c^2$. So, the exponent indicator in the distribution function includes additional factor $\varepsilon_i / T_i = (\varepsilon_i / m_i c^2) (T_i / m_i c^2)^{-1} = (\varepsilon_i / m_i c^2) (T_i / m_i c^2)^{-1}$. Functions $f_1(\chi_{e,i} \beta)$, $f_2(\chi_{e,i} \beta)$ and $f_3(\chi_{e,i} \beta)$ are calculated numerically below for the chosen values of temperatures. We introduce three characteristic velocities $\delta p_{e,i} = U_{pe}^2 \delta n_{e,i}$, $\delta \tilde{t}_{e,i} = U_{te,i}^2 \delta n_{e,i}$, and $\delta M_{e,i} = U_{Me,i}^4 \delta n_{e,i}$.

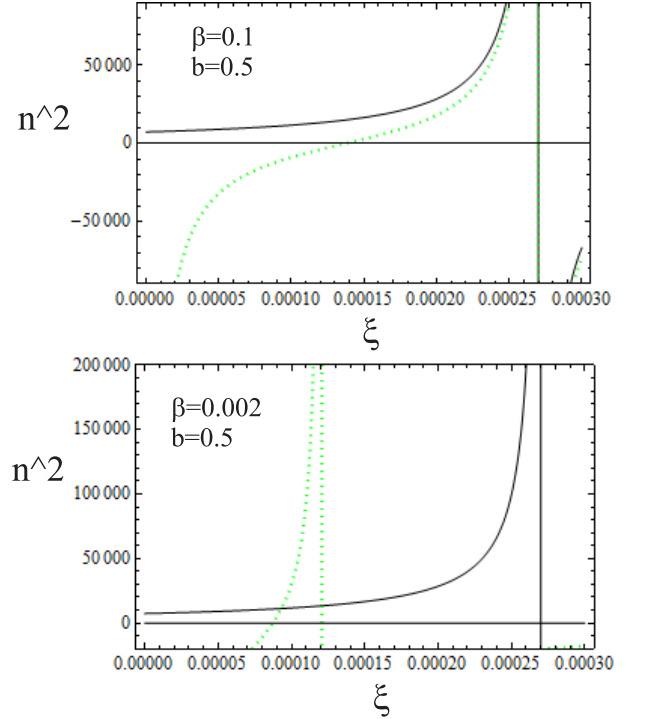


FIG. 3: The square of the refractive index of the Alfvénic waves is demonstrated. The further increase of temperature in compare with Fig. 2 is presented. Two temperatures are used for two plots in this figure $\beta = 0.1$ and $\beta = 0.002$.

The linearized equations have same structure for all species. Hence, equations for electrons and ions repeat equations presented for electrons in Ref. [23].

Let us present the expressions for the velocity field entering the linearized Maxwell equations

$$v_{xe,i} = \frac{i q_{e,i}}{m_{e,i}} \times$$

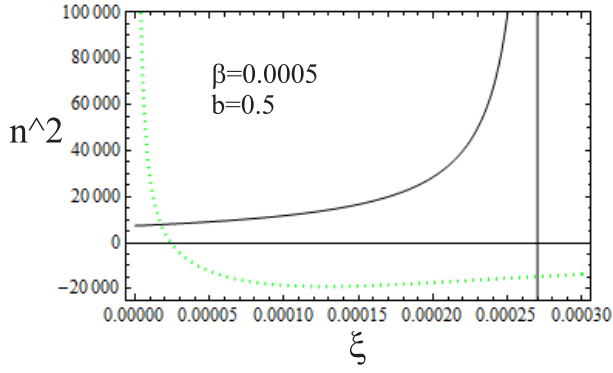


FIG. 4: The square of the refractive index of the Alfvénic waves is demonstrated. The further increase of temperature in compare with Fig. 3 is presented. One temperatures is used for this figure $\beta = 0.0005$.

$$\frac{\omega \left(\frac{\Gamma_{0e,i}}{n_{0e,i}} - \frac{U_{te,i}^2}{c^2} \right) \delta E_x - i \Omega_{e,i} \delta E_y \left(1 - \frac{5U_{pe,i}^2}{c^2} - \frac{10U_{Me,i}^4}{3c^4} \right)}{\omega^2 - \Omega_{e,i}^2 \left(1 - 5U_{pe,i}^2/c^2 \right)}, \quad (11)$$

and

$$v_{ye,i} = \frac{i q_{e,i}}{m_{e,i}} \times \frac{i \Omega_{e,i} \left(1 - \frac{5U_{pe,i}^2}{c^2} - \frac{10U_{Me,i}^4}{3c^4} \right) \delta E_x + \omega \left(\frac{\Gamma_{0e,i}}{n_{0e,i}} - \frac{U_{te,i}^2}{c^2} \right) \delta E_y}{\omega^2 - \Omega_{e,i}^2 \left(1 - 5U_{pe,i}^2/c^2 \right)}, \quad (12)$$

where $\Omega_e = -|\Omega_e| = q_e B_0 / m_e c$, $\Omega_i = |\Omega_i| = q_i B_0 / m_i c$ are the electron and ion cyclotron frequencies.

The linearized Maxwell equations are

$$(\omega^2 - k_z^2 c^2) \delta \mathbf{E} + 4\pi i \omega \sum_{s=e,i} q_s n_{0s} \delta \mathbf{v}_s = 0. \quad (13)$$

Using expressions of the velocity field via the electric field in equation (13) we obtain the equations for the projections of the electric field $\hat{\varepsilon} \delta \mathbf{E} = 0$:

$$\hat{\varepsilon} = \begin{pmatrix} \varepsilon_{xx} & \varepsilon_{xy} \\ \varepsilon_{yx} & \varepsilon_{yy} \end{pmatrix}, \quad (14)$$

where

$$\begin{aligned} \varepsilon_{xx} = \varepsilon_{yy} = & -\omega^2 + k^2 c^2 \\ & + \frac{\omega^2 \cdot \omega_{Le}^2}{\omega^2 - \Omega_e^2 (1 - 5U_{pe}^2/c^2)} \left(\frac{\Gamma_{0e}}{n_{0e}} - \frac{U_{te}^2}{c^2} \right) \\ & + \frac{\omega^2 \cdot \omega_{Li}^2}{\omega^2 - \Omega_i^2 (1 - 5U_{pi}^2/c^2)} \left(\frac{\Gamma_{0i}}{n_{0i}} - \frac{U_{ti}^2}{c^2} \right) \end{aligned} \quad (15)$$

and

$$\varepsilon_{xy} = (\varepsilon_{yx})^*$$

$$\begin{aligned} = & \frac{-i \omega \Omega_e \cdot \omega_{Le}^2}{\omega^2 - \Omega_e^2 (1 - 5U_{pe}^2/c^2)} \left(1 - \frac{5U_{pe}^2}{c^2} - \frac{10U_{Me}^4}{3c^4} \right) \\ & + \frac{-i \omega \Omega_i \cdot \omega_{Li}^2}{\omega^2 - \Omega_i^2 (1 - 5U_{pi}^2/c^2)} \left(1 - \frac{5U_{pi}^2}{c^2} - \frac{10U_{Mi}^4}{3c^4} \right) \end{aligned} \quad (16)$$

where $\omega_{Le}^2 = 4\pi e^2 n_0 / m_e$ is the electron Langmuir frequency, $\omega_{Li}^2 = 4\pi e^2 n_0 / m_i$ is the ion Langmuir frequency, and symbol (*) shows the complex conjugation.

A. Nonrelativistic limit

Let us prepare background for the analysis of the relativistically hot plasmas by consideration of the limit of small nonrelativistic temperatures. To this end, we neglect the thermal velocities U_p , U_t , U_M in compare with the speed of light in equations (14), (15), and (16). Hence, we obtain

$$\hat{\varepsilon}_{NR} =$$

$$\begin{pmatrix} k^2 c^2 - \omega^2 + \sum_s \frac{\omega^2 \cdot \omega_{Ls}^2}{\omega^2 - \Omega_s^2}, & \sum_s \frac{-i \Omega_s \omega \cdot \omega_{Ls}^2}{\omega^2 - \Omega_s^2} \\ \sum_s \frac{i \Omega_s \omega \cdot \omega_{Ls}^2}{\omega^2 - \Omega_s^2}, & k^2 c^2 - \omega^2 + \sum_s \frac{\omega^2 \cdot \omega_{Ls}^2}{\omega^2 - \Omega_s^2} \end{pmatrix}, \quad (17)$$

where $s = e, i$.

The dielectric permeability tensor (17) gives two expressions for the refractive index. We present one of them which includes the Alfvénic wave

$$n^2 = 1 - \frac{1}{\omega} \frac{\omega_{Le}^2}{\omega + |\Omega_e|} - \frac{1}{\omega} \frac{\omega_{Li}^2}{\omega - \Omega_i}. \quad (18)$$

The spectrum of nonrelativistic Alfvénic wave is located in area $\omega \in (0, \Omega_i)$. However, if we consider the limit $\omega \ll \Omega_i$ we get the famous expression

$$\omega^2 = \frac{k^2 v_A^2}{1 + v_A^2/c^2}, \quad (19)$$

where $v_A \equiv c \Omega_i / \omega_{Li}$ is the Alfvén velocity.

Expression (19) is obtained from (17) in the low frequency regime

$$\hat{\varepsilon}_{NR} =$$

$$\begin{pmatrix} k^2 c^2 - \omega^2 - \sum_s \frac{\omega^2 \cdot \omega_{Ls}^2}{\Omega_s^2}, & \sum_s \frac{i \omega \cdot \omega_{Ls}^2}{\Omega_s} \\ \sum_s \frac{-i \omega \cdot \omega_{Ls}^2}{\Omega_s}, & k^2 c^2 - \omega^2 - \sum_s \frac{\omega^2 \cdot \omega_{Ls}^2}{\Omega_s^2} \end{pmatrix}, \quad (20)$$

where $\varepsilon_{NR,xy} = \sum_s \frac{i \omega \cdot \omega_{Ls}^2}{\Omega_s} = 0$, and $\frac{\omega_{Le}^2}{\Omega_e^2} \ll \frac{\omega_{Li}^2}{\Omega_i^2}$ in $\varepsilon_{NR,xx}$ and $\varepsilon_{NR,yy}$.

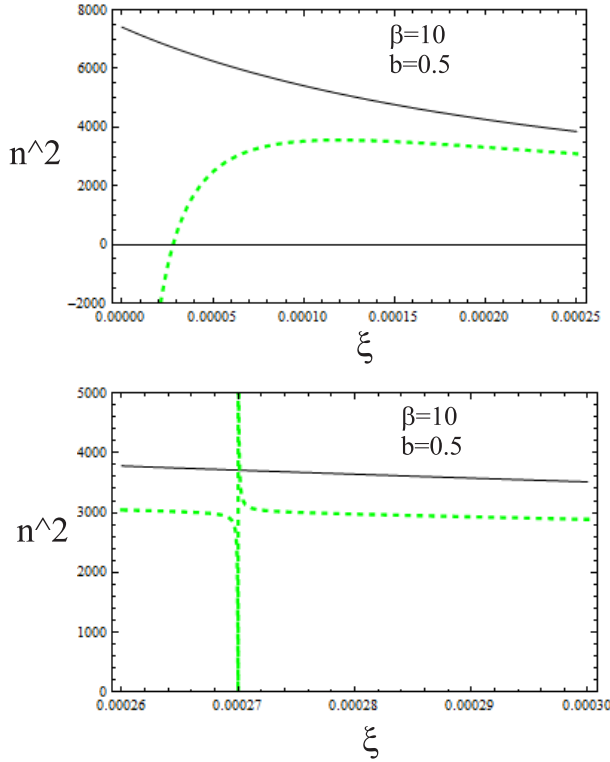


FIG. 5: The refractive index for the fast magneto-sound is presented. The continuous line presents the nonrelativistic result. The result of the relativistic model is presented with the dashed line. These notations are saved in other figures below. The reverse dimensionless temperature is shown in the plot.

B. Relativistic Alfvénic waves

Let us get back to the relativistic temperature regime. The refractive index for the Alfvénic waves following from equations (14), (15), (16) has the form presented below

$$\begin{aligned}
 n^2 = & 1 - \frac{1}{\omega} \frac{\omega_{Le}^2}{\omega^2 - \Omega_e^2 \left(1 - 5 \frac{U_{pe}^2}{c^2}\right)} \times \\
 & \times \left[\omega \left(\frac{\Gamma_{0e}}{n_{0e}} - \frac{U_{te}^2}{c^2} \right) - |\Omega_e| \left(1 - 5 \frac{U_{pe}^2}{c^2} - \frac{10U_{Me}^4}{3c^4} \right) \right] \\
 & - \frac{1}{\omega} \frac{\omega_{Li}^2}{\omega^2 - \Omega_i^2 \left(1 - 5 \frac{U_{pi}^2}{c^2}\right)} \times \\
 & \times \left[\omega \left(\frac{\Gamma_{0i}}{n_{0i}} - \frac{U_{ti}^2}{c^2} \right) + \Omega_i \left(1 - 5 \frac{U_{pi}^2}{c^2} - \frac{10U_{Mi}^4}{3c^4} \right) \right]. \quad (21)
 \end{aligned}$$

Equation (21) is a generalization of equation (18).

High frequency part of the refractive index $n(\omega)$, which is located near the ion-cyclotron frequency (the vertical

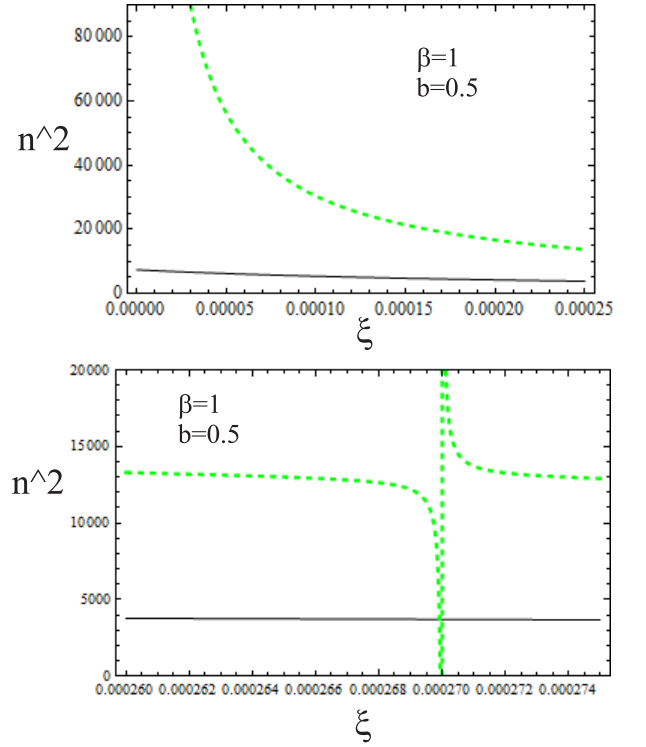


FIG. 6: The refractive index for the fast magneto-sound is given. More accurately, we have the curves for the low-frequency part of the fast extraordinary wave and the small frequency second branch. The continuous line presents the nonrelativistic result. The result of the relativistic model is presented with the dashed line.

line), shows small variation in compare with the nonrelativistic regime. Here, the relativistic effects show small increase of the refractive index. However, the transition to the small frequency are demonstrates the considerable increase of frequency. Moreover, the zero frequency limit is completely different. Instead of monotonic decrease of n at the decrease of frequency ω we see asymptotic growth to the infinity. It is related to the nonzero value of the nondiagonal elements of the dielectric permeability tensor. So, the pole at $\omega = 0$ is not canceled in this regime in contrast with the nonrelativistic limit.

Small increase of temperature from $\beta = 3$ to $\beta = 2$ and $\beta = 1$ shows a qualitative change of $n(\omega)$ in full area of existence of the Alfvénic wave. The increase of the refractive index demonstrated above changes to its considerable decrease. It happens due to the fact that $n(\omega)$ goes to zero at $\omega_0 \in (0, \Omega_i)$. The pole of $n(\omega)$ at $\omega = 0$ remains, but signature of $n^2(\omega)$ changes. All of it reveals in the decrease of the area of existence of the Alfvénic wave from $\omega \in (0, \Omega_i)$ to $\omega \in (\omega_0, \Omega_i)$. Same result can be found at the further increase of temperature $\beta = 0.1$ (see the upper plot in Fig. 3), where electrons getting in the ultrarelativistic regime, but ions are still in the nonrelativistic regime.

Parameter $\beta = 0.002$ corresponds to the ultrarelativis-

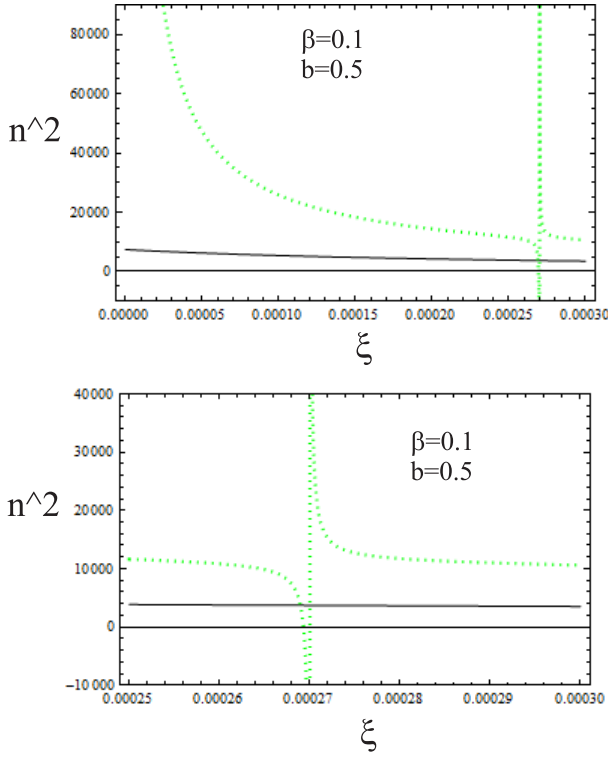


FIG. 7: The refractive index for the fast magneto-sound is obtained (the low-frequency part of the fast extraordinary wave and the small frequency second branch like on Fig. 6). The continuous line presents the nonrelativistic result. The result of the relativistic model is presented with the dashed line.

tic electrons and weakly relativistic ions (see the lower figure in Fig. 3). Relativistic temperature of ions reveals in the difference of the effective cyclotron frequency $\Omega_i \sqrt{1 - \frac{5U_{pe,i}^2}{c^2}}$ from the bare ion-cyclotron frequency Ω_i . Hence, the addition restriction of area of the Alfvénic wave existence appears. However, general picture of $n^2(\omega)$ is the same as at $\beta = 0.1$.

Fig. 4 is plotted for the regime of relativistically hot ions. Here, the effective cyclotron frequency square $\Omega_i^2(1 - \frac{5U_{pe,i}^2}{c^2})$ goes to small negative value. Area of existence of the Alfvénic wave disappear. However, there is a wave in area $\omega \in (0, \omega')$, where $\omega' \ll \Omega_i$. In its area of existence its $n(\omega)$ is similar to the small frequency part of the Alfvénic wave demonstrated in Fig. 1.

Therefore, three temperature regimes are found for the relativistic Alfvén waves in addition to the low (nonrelativistic) temperature regime.

C. Relativistic fast magneto-sound

High-frequency part of fast magneto-sound can be described with no account of ions. Corresponding result is shown in Ref. [23] for the relativistically hot electrons.

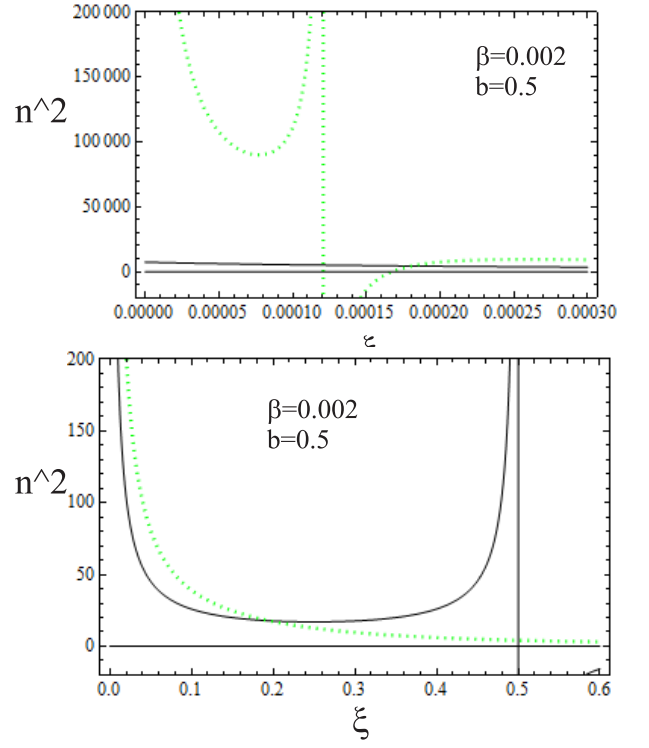


FIG. 8: The refractive index for the fast magneto-sound is presented which is actually replaced by the low-frequency part of the fast extraordinary wave and the small frequency second branch. The continuous line presents the nonrelativistic result. The result of the relativistic model is presented with the dashed line.

Ref. [23] demonstrates that $n \rightarrow +\infty$ at $\omega \rightarrow 0$ for fast magneto-sound at motionless ions. This pole shifts up to $\Omega_i \sqrt{1 - \frac{5U_{pe,i}^2}{c^2}}$ at the account of the relativistic ion motion (let us remind that $n(\omega = 0)$ has finite positive value for the nonrelativistic plasmas).

The refractive index for the relativistic fast magneto-sound including the relativistic ion motion is

$$\begin{aligned}
 n^2 = & 1 - \frac{1}{\omega} \frac{\omega_{Le}^2}{\omega^2 - \Omega_e^2(1 - 5\frac{U_{pe}^2}{c^2})} \times \\
 & \times \left[\omega \left(\frac{\Gamma_{0e}}{n_{0e}} - \frac{U_{te}^2}{c^2} \right) + |\Omega_e| \left(1 - 5\frac{U_{pe}^2}{c^2} - \frac{10U_{Me}^4}{3c^4} \right) \right] \\
 & - \frac{1}{\omega} \frac{\omega_{Li}^2}{\omega^2 - \Omega_i^2(1 - 5\frac{U_{pi}^2}{c^2})} \times \\
 & \times \left[\omega \left(\frac{\Gamma_{0i}}{n_{0i}} - \frac{U_{ti}^2}{c^2} \right) - \Omega_i \left(1 - 5\frac{U_{pi}^2}{c^2} - \frac{10U_{Mi}^4}{3c^4} \right) \right]. \quad (22)
 \end{aligned}$$

If the ion temperature is relatively small we have pole at Ω_i . This pole splits the area of existence of the fast

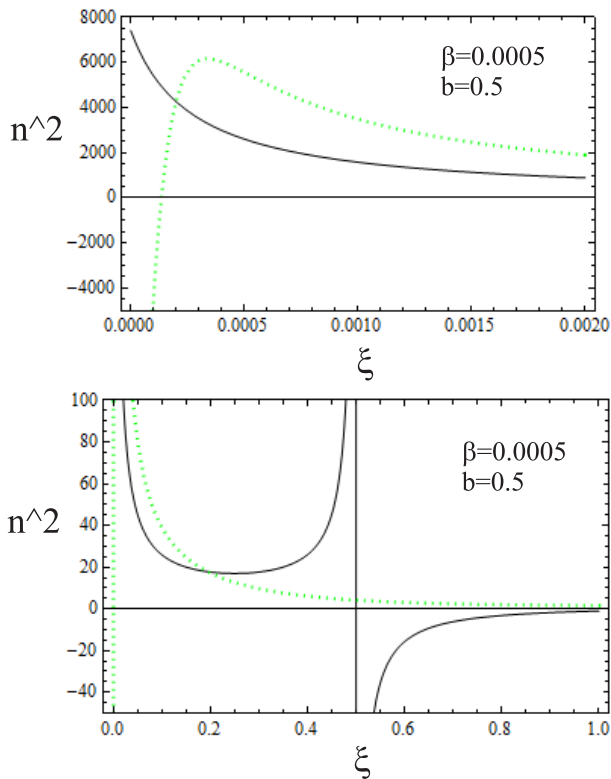


FIG. 9: The refractive index for the fast magneto-sound is shown, but in this regime it is completely replaced by the low-frequency part of the fast extraordinary wave. The continuous line presents the nonrelativistic result. The result of the relativistic model is presented with the dashed line.

magneto-sound on two areas separated by small interval of frequencies near Ω_i . Hence, we can conclude that there are two branches of waves instead of single fast magneto-sound. Frequencies of one wave is located below the effective cyclotron frequency $\Omega_i \sqrt{1 - \frac{5U_{pe,i}^2}{c^2}}$ (we call this wave the small frequency second branch). Frequency of the second wave is located above $\Omega_i \sqrt{1 - \frac{5U_{pe,i}^2}{c^2}}$. We associate it with the fast magneto-sound, since it has same high frequency limit of the fast magneto-sound.

Fig. 5 shows the result of numerical analysis of the refractive index for the fast magneto-sound. It demonstrates that the small relativistic temperature of electrons at almost nonrelativistic ions leads to the considerable change of the refractive index. The lower figure in Fig. 5 shows area near the ion cyclotron frequency Ω_i . The refractive index $n(\omega)$ has a pole here in the relativistic regime. There is small interval below the ion cyclotron frequency, where no wave exist. This area separate areas of existence of two waves. The fast magneto-sound is restricted from the small frequency area by the ion cyclotron frequency. The small frequency second branch appears in area $\omega \in (\tilde{\omega}, \Omega_i)$. For $\beta = 10$ we obtain $\tilde{\omega}/L_e = 0.00003$ as it is shown in the upper Fig. 5. Moreover, the refractive index in the relativistic regime

is smaller then the nonrelativistic the refractive index.

The second relativistic regime appears at $\beta = 1$ (see Fig. 6) and $\beta = 0.1$ (see Fig. 7). It modifies both the fast magneto-sound and the small frequency second branch. The fast magneto-sound wave exist below the effective electron cyclotron frequency, but its square is below zero. Hence, this area disappears. We have the low frequency part of the fast-extraordinary wave located at the frequency above the ion cyclotron frequency. The relativistic refractive index is larger then the refractive index in the nonrelativistic case. The small frequency second branch exists in area $\omega \in (0, \Omega_i)$, so the area is extended down to zero frequency. It corresponds to a small temperature part of the second relativistic regime found for the Alfvénic wave. However, four temperature regimes for the fast magneto-sound. So, the second relativistic regime found for the Alfvénic wave splits for two areas.

Further increase of temperature up to $\beta = 0.002$ shows further change of the low-frequency part of the fast extraordinary wave and the small frequency second branch. It corresponds to the small relativistic temperature effects on ions. So, the effective cyclotron frequency

$\Omega_i \sqrt{1 - \frac{5U_{pe,i}^2}{c^2}}$ is not changed in compare with Ω_i . The small frequency second branch shows further increase of the refractive index. Moreover, its behavior is changed near the ion cyclotron frequency. Tendency $n^2 \rightarrow -\infty$ is changed to $n^2 \rightarrow +\infty$. The refractive index of the fast extraordinary wave is also changed. In this regime, the minimal frequency of the fast extraordinary wave $\omega_{min} > \Omega_i$. Fig. 8 shows $\omega_{min}/\omega_{Le} = 0.00017$. At $\omega/\omega_{Le} \in (1.7 \times 10^{-4}, 1.85 \times 10^{-4})$ the refractive index of the fast extraordinary wave is smaller then frequency of the fast magneto-sound wave existing in the nonrelativistic limit. At larger frequencies $\omega/\omega_{Le} \in (1.85 \times 10^{-4}, 0.2)$ the refractive index of the fast extraordinary wave is larger then frequency of the fast magneto-sound wave.

Regime of relativistic ions with the temperature comparable with the rest energy of ion is presented in Fig. 9. Such large temperature leads to the negative square of the effective cyclotron frequency $\Omega_i^2 (1 - \frac{5U_{pe,i}^2}{c^2})$. Hence, there is no pole for this frequency. Therefore, the small frequency second branch existing below this frequency does not exist in this regime. We find the low-frequency part of the fast extraordinary wave only. The fast extraordinary wave exist at $\omega > \tilde{\omega}$. At $\beta = 0.0005$ we have $\tilde{\omega}/\omega_{Le} = 0.00015$. At $\omega/\omega_{Le} > 0.0002$ the refractive index of the fast extraordinary wave is above corresponding values for the nonrelativistic fast magneto-sound (see the upper Fig. 9). The lower Fig. 9 shows that such behavior goes up to $\omega/\omega_{Le} = 0.2$. At larger frequencies $\omega/\omega_{Le} \in (0.2, 0.5)$ the refractive index of the fast extraordinary wave is smaller in compare with the nonrelativistic fast magneto-sound.

IV. CONCLUSION

A dramatic change of the spectrum of the Alfvénic waves and fast magneto-sound has been found for the relativistically hot plasmas. First, these changes are crucial in compare with the nonrelativistic regime. Next, these changes are different for various relativistic regime which have been considered in the paper. More exactly, three relativistic regimes have been considered for the relativistically hot plasmas. These regimes corresponds to the different temperature intervals for the Alfvénic waves. Four regimes are found for different temperature intervals for the fast magneto-sound. Changes of spectra have been found. Modifications of areas of existence of waves have been obtained.

V. ACKNOWLEDGEMENTS

Work is supported by the Russian Foundation for Basic Research (grant no. 20-02-00476). This paper has been supported by the RUDN University Strategic Academic Leadership Program.

VI. DATA AVAILABILITY

Data sharing is not applicable to this article as no new data were created or analyzed in this study, which is a purely theoretical one.

Appendix A: Appendix A: Numerical estimation of the relativistic-thermal parameters for electrons

For the electrons we have $\chi_e = 1$, so $f_{1,2,3}(\chi_e\beta) = f_{1,2,3}(\beta)$.

Seven temperature regimes are chosen for the electrons $T_{e1} = 0.1m_e c^2$, $T_{e2} = m_e c^2$, $T_{e3} = 10m_e c^2$, $T_{e4} = 2 \times 10^3 m_e c^2$, $T_{e5} = 0.33m_e c^2$, $T_{e6} = 0.5m_e c^2$, and $T_{e7} = 0.5 \times 10^3 m_e c^2$. It gives the following values of the dimensionless reverse temperature $\beta = m_e c^2 / T_e$ and corresponding values of other parameters.

For the relatively small relativistic temperature $\beta_1 = 10$, we calculate $K_1/K_2 = 0.91$, $U_t^2/c^2 = 0.07$, $U_p^2/c^2 = 0.08$, and $U_M^4/c^4 = 0.02$, where $K_1(10) = 2 \times 10^{-5}$, $K_2(10) = 2.2 \times 10^{-5}$, $f_1(10) = 5 \times 10^{-7}$, $f_2(10) = 4.2 \times 10^{-7}$, $f_3(10) = 1.7 \times 10^{-7}$.

For $\beta_5 = 3$, we get $K_1/K_2 = 0.65$, $U_t^2/c^2 = \beta f_2/(3K_2) = 0.11$, $U_p^2/c^2 = \beta f_1/(3K_2) = 0.18$, and $U_M^4/c^4 = \beta f_3/(5K_2) = 0.07$, where $K_1(3) = 0.0402$, $K_2(3) = 0.062$, $f_1(3) = 0.011$, $f_2(3) = 0.0066$, $f_3(3) = 0.0071$.

For $\beta_6 = 2$, we get $K_1/K_2 = 0.55$, $U_t^2/c^2 = \beta f_2/(3K_2) = 0.11$, $U_p^2/c^2 = \beta f_1/(3K_2) = 0.22$, and $U_M^4/c^4 = \beta f_3/(5K_2) = 0.1$, where $K_1(2) = 0.14$,

$K_2(2) = 0.25$, $f_1(2) = 0.084$, $f_2(2) = 0.042$, $f_3(2) = 0.062$.

For $\beta_2 = 1$, we get $K_1/K_2 = 0.38$, $U_t^2/c^2 = \beta f_2/(3K_2) = 0.1$, $U_p^2/c^2 = \beta f_1/(3K_2) = 0.28$, and $U_M^4/c^4 = \beta f_3/(5K_2) = 0.15$, where $K_1(1) = 0.6$, $K_2(1) = 1.6$, $f_1(1) = 1.35$, $f_2(1) = 0.46$, $f_3(1) = 1.17$.

For $\beta_3 = 0.1$, we have $K_1/K_2 = 0.05$, $U_t^2/c^2 = \beta f_2/(3K_2) = 0.02$, $U_p^2/c^2 = 0.33$, and $U_M^4/c^4 = 0.2$, where $K_1(0.1) = 10$, $K_2(0.1) = 200$, $f_1(0.1) = 2 \times 10^3$, $f_2(0.1) = 100$, $f_3(0.1) = 2 \times 10^3$.

For $\beta_7 = 2 \times 10^{-3}$, we find $K_1/K_2 = 1 \times 10^{-3}$, $U_t^2/c^2 = \beta f_2/(3K_2) = 3.3 \times 10^{-4}$, $U_p^2/c^2 = \beta f_1/(3K_2) = 0.33$, and $U_M^4/c^4 = \beta f_3/(5K_2) = 0.2$, where $K_1(2 \times 10^{-3}) = 5 \times 10^2$, $K_2(2 \times 10^{-3}) = 5 \times 10^5$, $f_1(2 \times 10^{-3}) = 2.5 \times 10^8$, $f_2(2 \times 10^{-3}) = 2.5 \times 10^5$, $f_3(2 \times 10^{-3}) = 2.5 \times 10^8$.

For $\beta_4 = 0.5 \times 10^{-3}$, we find $K_1/K_2 = 0.25 \times 10^{-3}$, $U_t^2/c^2 = \beta f_2/(3K_2) = 8.3 \times 10^{-5}$, $U_p^2/c^2 = \beta f_1/(3K_2) = 0.33$, and $U_M^4/c^4 = \beta f_3/(5K_2) = 0.2$, where $K_1(5 \times 10^{-4}) = 2 \times 10^3$, $K_2(5 \times 10^{-4}) = 8 \times 10^6$, $f_1(5 \times 10^{-4}) = 1.6 \times 10^{10}$, $f_2(5 \times 10^{-4}) = 4 \times 10^6$, $f_3(5 \times 10^{-4}) = 1.6 \times 10^{10}$.

Appendix B: Appendix B: Numerical estimation of the relativistic-thermal parameters for ions

If we consider the isothermal plasmas $T_i = T_e$ we would also have seven temperature regimes.

However, functions $f_{1,2,3}(\chi_i\beta)$ depend on χ_i which should be calculated in each regime. Parameter $\chi_i = (m_i/m_e) \cdot (T_e/T_i)$ simplifies in the isothermal regime. $\chi_{i,I} = (m_i/m_e)$, where symbol I refers to the isothermal regime. Here, we consider the electron-proton or hydrogen plasmas. Hence, parameter $\chi_{i,I} = (m_i/m_e) = 1.84 \times 10^3$ is fixed. The argument of functions $f_{1,2,3}$ has the following values: $\chi_{i,I}\beta_1 = 1.84 \times 10^4$, $\chi_{i,I}\beta_2 = 1.84 \times 10^3$, $\chi_{i,I}\beta_3 = 1.84 \times 10^2$, and $\chi_{i,I}\beta_4 = 0.92$.

We start from the small temperature regime $\chi_{i,I}\beta_1 = 1.84 \times 10^4$, we calculate $K_1/K_2 = 0.99992$, $U_t^2/c^2 = 0$, $U_p^2/c^2 = \chi_{i,I}\beta f_1(\chi_{i,I}\beta)/(3K_2(\chi_{i,I}\beta)) = 0$, and $U_M^4/c^4 = 0$, where $f_1(1.84 \times 10^4) = 0$, $f_2(1.84 \times 10^4) = 0$, $f_3(1.84 \times 10^4) = 0$.

For $\chi_{i,I}\beta_2 = 1.84 \times 10^3$, we get $K_1/K_2 = 0.9992$, $U_t^2/c^2 = 0$, $U_p^2/c^2 = 0$, and $U_M^4/c^4 = 0$, where $f_1(1.84 \times 10^3) = 0$, $f_2(1.84 \times 10^3) = 0$,

For $\chi_{i,I}\beta_6 = 3.68 \times 10^3$, we get $K_1/K_2 = 0.9996$, $U_t^2/c^2 = 0$, $U_p^2/c^2 = 0$, and $U_M^4/c^4 = 0$, where $f_1(1.84 \times 10^3) = 0$, $f_2(1.84 \times 10^3) = 0$, $f_3(1.84 \times 10^3) = 0$.

For $\chi_{i,I}\beta_5 = 5.52 \times 10^3$, we get $K_1/K_2 = 0.9997$, $U_t^2/c^2 = 0$, $U_p^2/c^2 = 0$, and $U_M^4/c^4 = 0$, where $f_1(1.84 \times 10^3) = 0$, $f_2(1.84 \times 10^3) = 0$, $f_3(1.84 \times 10^3) = 0$.

For $\chi_{i,I}\beta_3 = 1.84 \times 10^2$, we have $K_1/K_2 = 0.992$, $U_t^2/c^2 = 5.3 \times 10^{-3}$, $U_p^2/c^2 = 5.3 \times 10^{-3}$, and $U_M^4/c^4 = 8.5 \times 10^{-5}$, where $K_1(1.84 \times 10^2) = 1.14 \times 10^{-81}$, $K_2(1.84 \times 10^2) = 1.2 \times 10^{-81}$, $f_1(1.84 \times 10^2) = 0$, $f_2(1.84 \times 10^2) = 0$, $f_3(1.84 \times 10^2) = 0$.

For $\chi_{i,I}\beta_4 = 0.92$ corresponding to temperature close to the rest energy of the proton, we have $K_1/K_2 = 0.35$, $U_t^2/c^2 = 0.09$, $U_p^2/c^2 = 0.28$, and $U_M^4/c^4 = 0.15$, where $K_1(0.92) = 0.69$, $K_2(0.92) = 1.98$, $f_1(0.92) = 1.82$, $f_2(0.92) = 0.58$, $f_3(0.92) = 1.6$.

For $\chi_{i,I}\beta_7 = 3.68$ corresponding to temperature close

to the rest energy of the proton, we have $K_1/K_2 = 0.7$, $U_t^2/c^2 = 0.1$, $U_p^2/c^2 = 0.16$, and $U_M^4/c^4 = 0.06$, where $K_1(3.68) = 1.8 \times 10^{-2}$, $K_2(3.68) = 2.6 \times 10^{-2}$, $f_1(3.68) = 3.4 \times 10^{-3}$, $f_2(3.68) = 2.2 \times 10^{-3}$, $f_3(3.68) = 2 \times 10^{-3}$.

-
- [1] A. D. Turnbull, E. J. Strait, W. W. Heidbrink, M. S. Chu, H. H. Duong, J. M. Greene, L. L. Lao, T. S. Taylor, and S. J. Thompson, "Global Alfvén modes: Theory and experiment", *Physics of Fluids B: Plasma Physics* (1989-1993) **5**, 2546 (1993).
- [2] S. M. Mahajan, D. W. Ross, and GwoLiang Chen, "Discrete Alfvén eigenmode spectrum in magnetohydrodynamics", *Physics of Fluids* (1958-1988) **26**, 2195 (1983).
- [3] C. K. Goertz, "Kinetic Alfvén waves on auroral field lines", *Planet. Space Sci.*, **32**, 1387 (1984).
- [4] P. Louarn, J. E. Wahlund, T. Chust H. de Feraudy. A. Roux, B. Holback, P. O. Dovner, A. I. Eriksson and G. Holmgren, "Observation of kinetic Alfvén waves by the FREJA spacecraft", *Geophysical Research Letters*, **21**, 1847, (1994).
- [5] M. Volwerk, P. Louarn, T. Chust, A. Roux, H. de Feraudy, B. Holback, "Solitary kinetic Alfvén waves: A study of the Poynting flux", *Journal of Geophysical Research*, **101**, 13,335 (1996).
- [6] F. Mottez, V. Genot, "Electron acceleration by an Alfvénic pulse propagating in an auroral plasma cavity", *J. Geophys. Res.*, **116**, A00K15 (2011).
- [7] V. Genot, E. Mottez, and P. Louarn "Particle Acceleration Linked to Alfvén Wave Propagation on Small Scale Density Gradients", *Phys. Chem. Earth*, **26**, 219 (2001).
- [8] F. Mottez, "Plasma acceleration by the interaction of parallel propagating Alfvén waves", *J. Plasma Phys.* **81**, 325810104 (2015)
- [9] C. C. Chaston, C. W. Carlson, W. J. Peria, R. E. Ergun, J. P. McFadden, "FAST Observations of Inertial Alfvén Waves in the Dayside Aurora", *Geophysical Research Letters* **26**, 647 (1999).
- [10] D. W. Ross, G. L. Chen, and S. M. Mahajan, "Kinetic description of Alfvén wave heating", *Phys. Fluids* **25**, 652 (1982).
- [11] A. Hasegawa and L. Chen, "Kinetic Process of Plasma Heating Due to Alfvén Wave Excitation", *Phys. Rev. Lett.* **35**, 370 (1975).
- [12] S. D. Bale, P. J. Kellogg, F. S. Mozer, T. S. Horbury, and H. Reme, "Measurement of the Electric Fluctuation Spectrum of Magnetohydrodynamic Turbulence", *Phys. Rev. Lett.* **94**, 215002 (2005).
- [13] F. Sahrtaoui, M. L. Goldstein, P. Robert, and Yu. V. Khotyaintsev, "Evidence of a Cascade and Dissipation of Solar-Wind Turbulence at the Electron Gyroscale", *Phys. Rev. Lett.* **102**, 231102 (2009).
- [14] W. Gekelman, S. Vincena, B. Van Compernelle, G. J. Morales, J. E. Maggs, P. Pribyl, and T. A. Carter, "The many faces of shear Alfvén waves", *Phys. Plasmas* **18**, 055501 (2011).
- [15] W. Gekelman, P. Pribyl, S. Vincena, S. W. Tang, and K. Papadopoulos, "Ferrite based antennae for launching Alfvén waves", *Review of Scientific Instruments* **90**, 083505 (2019).
- [16] S. Dorfman and T. A. Carter, "Non-linear Alfvén wave interaction leading to resonant excitation of an acoustic mode in the laboratory", *Phys. Plasmas* **22**, 055706 (2015).
- [17] R. D. Hazeltine, S. M. Mahajan, "Fluid description of relativistic, magnetized plasma", *The Astrophysical Journal* **567**, 1262 (2002).
- [18] S. M. Mahajan, R. D. Hazeltine, "Fluid description of a magnetized plasma", *Phys. Plasmas* **9**, 1882 (2002).
- [19] N. L. Shatashvili, J. I. Javakhishvili, H. Kaya, "Nonlinear wave dynamics in two-temperature electron-positron-ion plasma", *Astrophys Space Sci.* **250**, 109 (1997).
- [20] N. L. Shatashvili and N. N. Rao, "Localized nonlinear structures of intense electromagnetic waves in two-temperature electron-positron-ion plasmas", *Phys. Plasmas* **6**, 66 (1999).
- [21] N. L. Shatashvili, S. M. Mahajan, and V. I. Berezhiani, "Nonlinear coupling of electromagnetic and electron acoustic waves in multi-species degenerate astrophysical plasma", *Phys. Plasmas* **27**, 012903 (2020).
- [22] P. A. Andreev, "On the structure of relativistic hydrodynamics for hot plasmas", arXiv:2105.10999.
- [23] P. A. Andreev, "Waves propagating parallel to the magnetic field in relativistically hot plasmas: A hydrodynamic models", arXiv:2106.14327.
- [24] P. A. Andreev, "On a hydrodynamic description of waves propagating perpendicular to the magnetic field in relativistically hot plasmas", arXiv:2107.13603.
- [25] L. S. Kuz'menkov, "Field form of dynamics and statistics of systems of particles with electromagnetic interaction", *Theoretical and Mathematical Physics* **86**, 159 (1991).
- [26] M. A. Drofa, L. S. Kuz'menkov, "Continual approach to multiparticle systems with long-range interaction. Hierarchy of macroscopic fields and physical consequences", *Theoretical and Mathematical Physics* **108**, 849 (1996).
- [27] L. S. Kuz'menkov and P. A. Andreev, "Microscopic Classic Hydrodynamic and Methods of Averaging", presented in PIERS Proceedings, p. 158, August 19-23, Moscow, Russia 2012.
- [28] S. Weinberg, *Gravitation and Cosmology* (John Wiley and Sons, Inc., New York, 1972).